Available online at www.sciencedirect.com
ScienceDirect
Colloids and Surfaces A: Physicochem. Eng. Aspects 300 (2007) 60–64
COLLOIDS AND SURFACES A
www.elsevier.com/locate/colsurfa

Monte Carlo study on the water bridge that produces the pull-off force in atomic force microscopy

Joonkyung Jang [a,*], Jonggu Jeon [b], Sungu Hwang [c]

[a] *Department of Nanomaterials Engineering and BK21 Nanofusion Technology Team, Pusan National University, Miryang 627-706, Republic of Korea*
[b] *Complex Fluids Laboratory, Korea Institute of Science and Technology, Seoul 136-791, Republic of Korea*
[c] *Department of Nanomedical Engineering and BK21 Nanofusion Technology Team, Pusan National University, Miryang 627-706, Republic of Korea*

Received 18 June 2006; received in revised form 15 December 2006; accepted 17 January 2007
Available online 21 January 2007

Abstract

A lattice gas model is implemented in simulating nanoscale water bridges condensed between a silicon nitride tip and a mica surface. We demonstrate how to calculate the pull-off force on the tip by using a Monte Carlo method. For four different tips, we checked how the width of a water bridge varies with respect to humidity. We also investigate the correlation between the bridge width and pull-off force.

Keywords: Monte Carlo; Pull-off force; Atomic force microscopy; Capillary condensation; Lattice gas

1. Introduction

In a typical atomic force microscopy (AFM) [1–3], a water bridge condenses between the AFM tip and a sample surface. This capillary condensation gives rise to a large adhesion force between the tip and sample. In the case of a silicon nitride tip interacting with a mica surface, several experimental groups have reported the pull-off force (the force needed to pull away a tip initially touching a sample surface) [1–3]. Unfortunately, there is no consensus on how the force depends on humidity. Sedin and Rowlen [1] and Thundat et al. [2] observed a flat response of pull-off force below 20% humidity and a monotonic increase that persists up to 80% humidity. In contrast, Salmeron and co-workers [3] reported a small, constant force at humdities less than 20%, a dramatic increase near 20% humidity and then a maximal force at 25–30% followed by a gradual decrease. We pointed out that the above discrepancy might be due to the difference in tip shape used in experiments. Our Monte Carlo simulation showed a slight difference in tip shape can make a drastic change in the pull-off force [4].

The pull-off force arises from the water bridge. However, little is known about how this nanoscale liquid bridge is related to the pull-off force. Thermodynamic theories, such as the Kelvin equation [5,6] have been routinely adopted to explain the bridge shape and the resulting pull-off force. However, applicability of thermodynamics for a nanometer-sized water bridge is questionable because it often shows a large fluctuation in its periphery [7,8]. Here, we use Monte Carlo simulations to study systematically the water bridge by changing the tip–sample distance and humidity. Using a thermodynamic integration method, we calculate pull-off forces for four different tips. Previously, we have shown that the width of the bridge is a fundamental variable which indicates the occurrence of a capillary condensation [8] and the stability of the water bridge [7]. Here, we investigate the relation between the bridge width and the pull-off force. There has been much work on the Monte Carlo simulation of the formation and snap-off of liquid junction between solid surfaces [6,9–11]. Unfortunately, the geometries considered in such work are mostly slits or cylinders, which are not relevant to an AFM tip on a surface.

2. Theory and calculation

2.1. System geometry and energy parameters of simulation

The present Monte Carlo simulation is based on a lattice gas model [12,13]. Our system is a spherical AFM tip close to a

* Corresponding author. Tel.: +82 55 350 5277; fax: +82 55 350 5837.
E-mail address: jkjang@pusan.ac.kr (J. Jang).

0927-7757/$ – see front matter © 2007 Elsevier B.V. All rights reserved.
doi:10.1016/j.colsurfa.2007.01.024

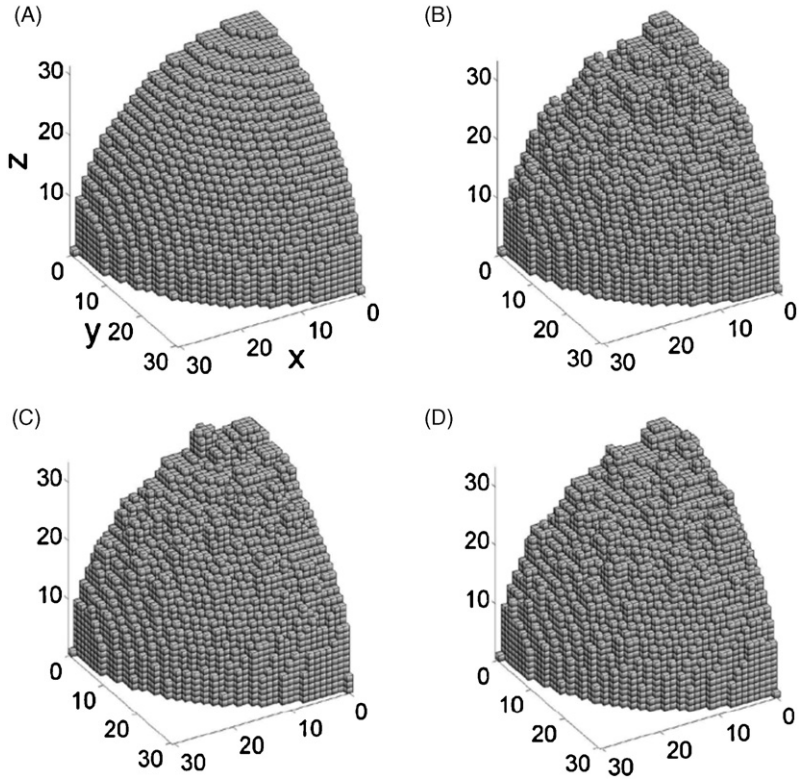

Fig. 1. Four tips considered in our Monte Carlo simulation. Tip A is a smooth spherical tip and the other tips have root-mean-square roughness of about 0.2 nm. Only the first quadrants of tips are shown. In this and the next figures, lengths are in the unit of lattice spacing, l (=0.37 nm).

flat sample surface. We have considered the same set of tips as in our previous work [4]: a smooth spherical tip (A), and three rough tips drawn in Fig. 1. Tips are shown upside down for visual clarity. The root-mean-square roughness for tips B, C, and D are 0.22 nm, 0.21 nm, and 0.19 nm, respectively. Due to small roughness, tips are not much different from each other. Water molecules can occupy cubic lattice sites confined between the tip and sample. Lengths are in the unit of *lattice spacing*, l. In physical dimensions, the lattice spacing is taken to be the molecular diameter of water, 0.37 nm [14]. The horizontal range of our system is $-30 \le x$, $y \le 30$. Only first quadrant ($x \ge 0$, $y \ge 0$) of the system is shown in the figure, and the remaining quadrants are taken to be mirror images of the first quadrant with respect to the *XZ*- and *YZ*-planes, and the *Z*-axis. Invoking this reflecting boundary condition yields nearly identical results to simulations that include the complete system. The flat sample surface is a square lattice located at $Z = 0$.

A water molecule interacts with its nearest neighbor molecules with attraction energy ε and has its own chemical potential μ. When it is located at one of the nearest neighbor sites of the tip and sample surfaces, it feels binding energies, b_T and b_S, respectively. The system Hamiltonian is then

$$H = -\varepsilon \sum_{i,j=nn} c_i c_j - b_T \sum_{i=\text{tip surf.}} c_i - b_S \sum_{i=\text{sample surf.}} c_i - \mu N, \quad (1)$$

where c_i is the occupancy (1 or 0) of the ith site, and the first summation runs over nearest neighbor pairs, the second is for the sites next to the tip surface, and the third for the sites right next to the sample surface. N is the number of molecules in the system. Energetic parameters, b_T/ε and b_S/ε, are chosen to mimic a silicon nitride tip interacting with a mica surface. The tip binding energy, b_T, is taken from the heat of adsorption for a water on a silicon nitride tip (=50 kJ/mol [15]). The binding energy of water on mica, b_S, is taken from the ab initio calculation by Odelius et al. (46 kJ/mol [16]). By dividing the above values by a hydrogen bonding strength (18.63 kJ/mol) [17], we get $b_T/\varepsilon = 2.68$ and $b_S/\varepsilon = 2.47$. Humidity is defined as $\exp[(\mu - \mu_C)/k_B T]$, where μ is chemical potential and μ_C (=-3ε) is the chemical potential at the bulk gas–liquid transition. This definition is the ideal gas limit expression for the system pressure relative to the bulk saturation pressure. The bulk critical temperature in our lattice model is exactly known as $k_B T_C/\varepsilon = 1.128$ [13]. Therefore, the water–water attraction is automatically set to be $\varepsilon = 4.771$ kJ/mol because $T_C = 647.30$ K. Temperature in our simulation is fixed at room temperature (300 K), $T/T_C = 0.46$. If we use the above physical values for ε and l, our force unit is $\varepsilon/l = 0.021$ nN. Using the above interaction and thermodynamic parameters and the Hamiltonian Eq. (1), we performed grand canonical (μVT) Monte Carlo simulations by following the procedure detailed elsewhere [18,19].

2.2. Computation of the width of water bridge and pull-off force

The width of a water bridge is defined as the width at its waist [Fig. 2(a)]. We first generated many (typically 50,000) equilib-

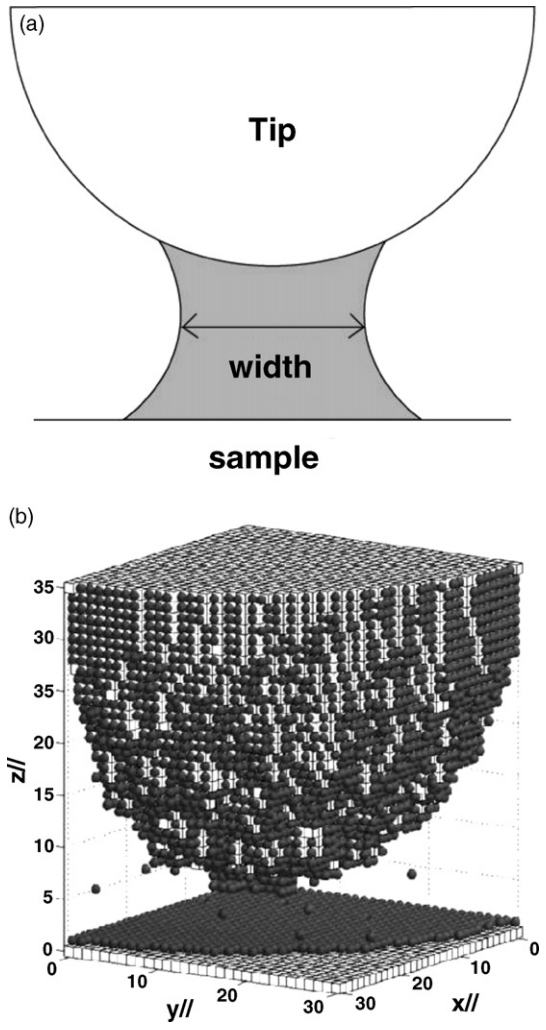

Fig. 2. (a) A schematic diagram illustrating the water bridge condensed between an AFM tip and a sample surface. The width of a concave bridge is defined as its waist width. (b) A simulated snapshot of water molecules condensed between an AFM tip and a flat sample. Water molecules are drawn as spheres. Tip and sample surface sites are represented as cubes. Relative humidity is set to 40% and the tip–sample distance, h, is three lattice spacings. Only the first quadrant ($x \geq 0$, $y \geq 0$) of our system is shown.

rium configurations by using a Monte Carlo method. Fig. 2(b) is a typical equilibrium configuration obtained this way. For each configuration, we counted the number of columns which are continuously occupied with water molecules. This guarantees the width is measured at the waist of a concave bridge. The collection of such columns looks like a circle when viewed along the Z-axis (perpendicular to the sample surface). We define the circle diameter as the bridge width for that configuration. We averaged the above diameter over 50,000 different equilibrium configurations.

The adhesion force, F, at a given tip–sample distance, h, is calculated by using the following relation [20],

$$\left(\frac{\partial F}{\partial \mu}\right)_{h,T} = \left(\frac{\partial N_{\mathrm{ex}}}{\partial h}\right)_{\mu}, \tag{2}$$

where N_{ex} is the excess number of molecules with respect to that of bulk ($N_{\mathrm{ex}} = N - N_{\mathrm{bulk}}$). The capillary force $F(h)$ is obtained by integrating Eq. (2) with respect to chemical potential μ. The integral form of Eq. (2) is given by

$$F(\mu, h, T) - F(-\infty, h, T) = \int_{-\infty}^{\mu} \left(\frac{\partial N_{\mathrm{ex}}}{\partial h}\right)_{\mu'} \mathrm{d}\mu'. \tag{3}$$

Starting from a sufficiently low μ that gives zero values for $(\partial N_{\mathrm{ex}}/\partial h)$, we discretized the integral in Eq. (3) by using Simpson's rule and evaluating $(\partial N_{\mathrm{ex}}/\partial h)$ at intermediate μ values. The derivative with respect to h in Eq. (2) is evaluated as $\partial N_{\mathrm{ex}}/\partial h = [N_{\mathrm{ex}}(h+l) - N_{\mathrm{ex}}(h)]/l$, where $N_{\mathrm{ex}}(x)$ is the excess number at a tip–sample distance x. We calculate the bulk density ($\rho = N_{\mathrm{bulk}}/V$, V = volume) by using the mean-field density functional theory (DFT) [21]. Within the DFT, the grand potential per unit volume is given by

$$\frac{\Omega_{\mathrm{DFT}}}{V} = k_{\mathrm{B}}T[\rho \log\rho - (1-\rho)\log(1-\rho)] - 3\varepsilon\rho^2 - \mu\rho, \tag{4}$$

where ρ is the density. The equilibrium density is determined by the condition, $\delta(\Omega_{\mathrm{DFT}}/V)/\delta\rho = 0$. We confirmed the accuracy of the DFT by running several simulations for the bulk system. At a given humidity, we calculated $F(h)$ for each tip.

3. Results and discussion

3.1. Humidity dependence on the water bridge width

In Fig. 2(b), we plot a snapshot of water molecules condensed between a rough tip and a flat sample surface at a relative humidity of 40%. The snapshot is one of many equilibrium configurations generated by using the Monte Carlo method described earlier. Note the tip is completely covered with water molecules whereas the mica-like sample surface is partially and cylindrically covered around the tip. The tip–sample distance, h, is 1.11 nm in this case. Unlike its macroscopic counterpart, this nanometer water bridge shows a substantial fluctuation in its width (typically about 5% of its average width).

For each humidity considered in the simulation, we calculated the capillary force F of each tip as a function of tip–sample distance h. Typically, $F(h)$ is attractive when the tip is close to the sample ($h < 1.2$ nm). As h increases, F eventually approaches zero. From $F(h)$ curve, we identified the pull-off force as the magnitude of the maximal attractive force. And the distance which gives that pull-off force is taken to be the pull-off distance. In all the cases considered in our simulation, the pull-off distance was either $h = l$ (0.37 nm) or $h = 2l$ (0.74 nm). Fig. 3 illustrates how the width of a water bridge responds to varying humidity. Note the width in the figure corresponds to the one at the pull-off distance. One can see that, overall, the bridge width increases with raising humidity. But for tips B and D, there is a sudden drop in the width near humidities 40 and 5%, respectively. This abrupt drop is due to the fact that the pull-off distance has increased from $h = l$ (0.37 nm) to $h = 2l$ (0.74 nm). As the bridge width is smaller for a larger h (because the molecules are less confined), the bridge width at the pull-off distance shows a discontinuity as in Fig. 3. However, for a fixed h, the sorption curve (N versus humidity) is continuous. Once the pull-off distance has increased to $h = 2l$ (0.74 nm), the bridge width increases with a humidity

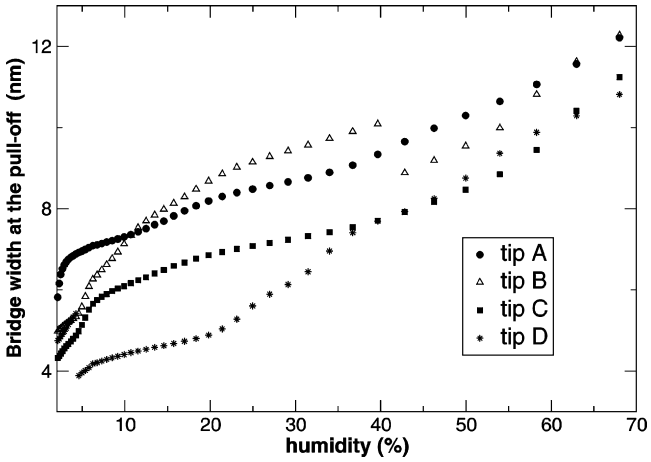

Fig. 3. The liquid bridge width vs. relative humidity. For four different tips, we examined the bridge width at the tip–surface distance that gives rise to the maximal attractive force. Overall, the bridge width increases with raising humidity. A sudden drop in the width for tips B and D is due to the fact that the pull-off distance has increased from $h = l$ to $h = 2l$.

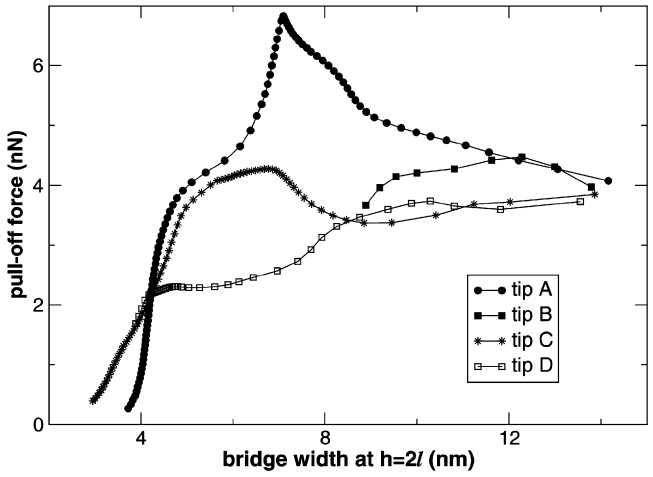

Fig. 5. Pull-off force vs. the bridge width for four tips considered in this work. The pull-off distance is $2l$ in this case. Compared to the pull-off distance $h = l$, the pull-off force is significantly non-linear with respect to the bridge width variation.

rise. Notice, at low humidities (<30%), the bridge width is wildly different for each tip. It is surprising that such a slight difference in the tip shape results in a drastic change in the bridge width. As humidity approaches 70%, the bridge width becomes similar to each other (but it is not identical).

3.2. Correlation between water bridge and pull-off force

We now investigate the correlation between the pull-off force and the bridge width. In Fig. 4, the pull-off force is plotted as a function of bridge width at the pull-off distance of $h = l$ (0.37 nm). One can see that the pull-off force rises with raising the bridge width. Then we might think that a wider bridge means a larger adhesion energy of it, giving a stronger attractive force. This is misleading however because, for tip B, the force actually decreases with increasing the bridge width above 9.5 nm. It is also interesting that the bridge width is remarkably different from each other even though all the four tips are similar in shape. This illustrates the water bridge shape is very sensitive to the atomic details of the tip.

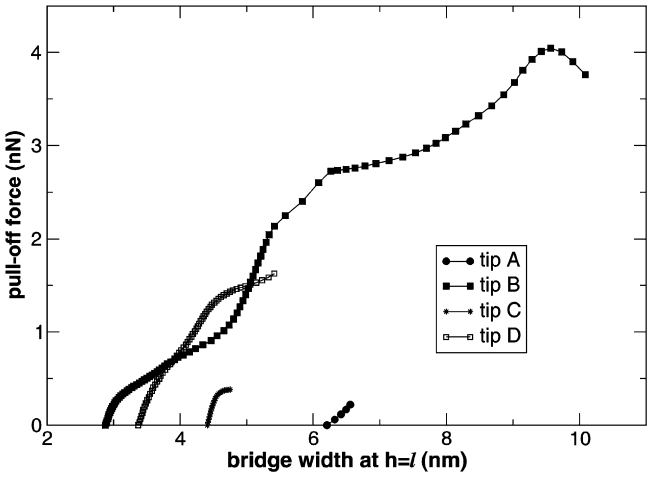

Fig. 4. Pull-off force vs. the water bridge width at a pull-off distance of l. On the whole, the pull-off force is proportional to the bridge width. For tip B however, the pull-off force starts to decrease with increasing the width above 9.5 nm.

The pull-off force versus the bridge width for the pull-off distance of $h = 2l$ (0.74 nm) is plotted in Fig. 5. A non-monotonic dependence of the force on the bridge width is more prominent in this case. The force begins to decrease with respect to the bridge width, starting at a width about 7 nm for tips A and C. The pull-off force of tip B starts to decline at a much larger value of the width (~12 nm). Tip D shows a nearly monotonically increasing force with respect to the width. Comparison of Figs. 5 and 4 illustrates that the dependence of the pull-off force on the bridge width changes dramatically by changing the pull-off distance. Therefore, the tip–sample distance is another important variable in determining the pull-off force.

4. Conclusions

We have simulated nanoscopic water bridges that form in atomic force microscopy. This nanoscopic bridge reacts sensitively to the atomic details of the tip geometry. Our calculation (0–7 nN) faithfully reproduces the order of magnitude of the experimental force. For small water bridges (width less than 7 nm), the pull-off force increases with enhancing the water bridge width for all the tips considered in this work. Further increasing the bridge width can lead to a decrease in the pull-off force depending on the tip shape. It is hard to find the definitive relationship between the pull-off force and the water bridge width. In order to understand the pull-off force, we might need to take into account the pull-off distance and the shape of the tip as well.

Acknowledgements

This work was supported by the Korea Research Foundation Grant funded by the Korean Government (MOEHRD, Basic

Research Promotion Fund) (Grant No. 2005-070-C00065). J. Jang thanks Dr. Sui-Rhane Chung for preparation of figures.

References

[1] D.L. Sedin, K.L. Rowlen, Anal. Chem. 72 (2000) 2183.
[2] T. Thundat, X.Y. Zheng, G.Y. Chen, R.J. Warmack, Surf. Sci. Lett. 294 (1993) L939.
[3] J. Hu, X.D. Xiao, D.F. Ogletree, M. Salmeron, Science 268 (1995) 267.
[4] J. Jang, M.A. Ratner, G.C. Schatz, J. Phys. Chem. B 110 (2006) 659.
[5] L.R. Fisher, J.N. Israelachvili, J. Colloid Interface Sci. 80 (1981) 528.
[6] L.D. Gelb, K.E. Gubbins, R. Radhakrishnan, M. Sliwinska-Bartkowiak, Rep. Prog. Phys. 62 (1999) 1573.
[7] J. Jang, G.C. Schatz, M.A. Ratner, Phys. Rev. Lett. 92 (2004) 085504.
[8] J. Jang, G.C. Schatz, M.A. Ratner, J. Chem. Phys. 116 (2002) 3875.
[9] A. Vishnyakov, A.V. Neimark, J. Chem. Phys. 119 (2003) 9755.
[10] S. Sacquin-Mora, A.H. Fuchs, Phys. Rev. E 68 (2003) 066103.
[11] W. Gac, A. Patrykiejew, S. Sokolowski, Surf. Sci. 318 (1994) 318.
[12] T. Hill, Statistical Mechanics, McGraw-Hill, New York, 1956.
[13] R. Pandit, M. Schick, M. Wortis, Phys. Rev. B 26 (1982) 5112.
[14] L. Maibaum, D.A. Chandler, J. Phys. Chem. B 107 (2003) 1189.
[15] B. Fubini, M. Volante, V. Bolis, E. Giamello, J. Mater. Sci. 24 (1989) 549.
[16] M. Odelius, M. Bernasconi, M. Parrinello, Phys. Rev. Lett. 78 (1997) 2855.
[17] S.J. Grabowski, Chem. Phys. Lett. 338 (2001) 361.
[18] J. Jang, G.C. Schatz, M.A. Ratner, J. Chem. Phys. 120 (2004) 1157.
[19] J. Jang, G.C. Schatz, M.A. Ratner, Phys. Rev. Lett. 90 (2003) 156104.
[20] S.G. Ash, D.H. Everett, C. Radke, Faraday Trans. II 69 (1973) 1256.
[21] M.J. De Oliveira, R.B. Griffiths, Surf. Sci. 71 (1978) 687.